Efficient Computation of Extended Surface Sources

William W. Symes
Department of Computational and Applied Mathematics,
Rice University,Houston TX 77251-1892 USA,
email symes@rice.edu,
ORCID 0000-0001-6213-4272

ABSTRACT

Source extension is a reformulation of inverse problems in wave propagation, that at least in some cases leads to computationally tractable iterative solution methods. The core subproblem in all source extension methods is the solution of a linear inverse problem for a source (right hand side in a system of wave equations) through minimization of data error in the least squares sense with soft imposition of physical constraints on the source via an additive quadratic penalty. A variant of the time reversal method from photoacoustic tomography provides an approximate solution that can be used to precondition Krylov space iteration for rapid convergence to the solution of this subproblem. An acoustic 2D example for sources supported on a surface, with a soft contraint enforcing point support, illustrates the effectiveness of this preconditioner.

Keywords: inverse problems, wave propagation, time reversal, Krylov subspace methods, preconditioning

INTRODUCTION

Full Waveform Inversion (FWI) can be described in terms of

1. a linear wave operator $L[\mathbf{c}]$, depending on a vector of space-dependent coefficients $\mathbf{c}$ and acting on causal vector wavefields $\mathbf{u}$ vanishing in negative time:

$$\mathbf{u} \equiv 0, t \ll 0; \tag{1}$$

2. a trace sampling operator P acting on wavefields and producing data traces;

3. and a (vector) source function (of space and time) $\mathbf{f}$ representing energy input to the system.

The basic FWI problem is: given data d, find $\mathbf{c}$ so that data is fit and wave physics are honored, that is,

$$P\mathbf{u} \approx d \text{ and } L[\mathbf{c}]\mathbf{u} = \mathbf{f}. \tag{2}$$

The source function $\mathbf{f}$ may be given, or to be determined along with $\mathbf{c}$. The task 2 may be cast as a nonlinear least squares problem:

$$\text{choose } \mathbf{c} \text{ to minimize } \|PL[\mathbf{c}]^{-1}\mathbf{f} - d\|^2. \tag{3}$$

Practical variants of the least squares problem 3 typically augment the objective with additive penalties or other constraints (Virieux and Operto, 2009; Fichtner, 2010; Schuster, 2017).

As is well-known, local optimization methods are the only feasible approach given the dimensions of a typical instance of 2, and those have a tendency to stall at uninformative model estimates due to "cycle-skipping". This phenomenon is often interpreted as the capture of optimizing sequences at local minima of the nonlinear objective function in 3 far from the global minimum, or at least not possessing the characteristics of a useful solution. See for example Gauthier et al. (1986); Virieux and Operto (2009); Pladys et al. (2021).

Source extension is one approach to avoiding this"cycle-skipping" obstacle. It consists in imposing the wave equation as a soft constraint, allowing the source field $\mathbf{f}$ to have more degrees of freedom than is permitted by a faithful model model of the seismic experiment, and constraining these additional degrees of freedom by means of an additive quadratic penalty modifying the problem 3:

$$\text{choose } \mathbf{c}, \mathbf{f} \text{ to minimize } \|PL[\mathbf{c}]^{-1}\mathbf{f} - d\|^2 + \alpha^2\|A\mathbf{f}\|^2 \tag{4}$$

The linear operator A penalizes deviation from known (or assumed) characteristics of the source function - its null space consists of feasible (or "physical") source models.

Well-studied examples of extended source approaches to FWI include Wavefield Reconstruction Inversion (WRI) (van Leeuwen and Herrmann, 2013, 2016; Li et al., 2018; Aghmiry et al., 2020; Louboutin et al., 2020) and Adaptive Waveform Inversion (AWI) (Warner and Guasch, 2016; Guasch et al., 2019, 2020; Yong et al., 2021; Warner et al., 2021). Huang et al. (2019) present an overview of the recent literature on source extension methods.

The present paper concerns *surface source extension*: physical sources are presumed to be concentrated at points in space, whereas their extended counterparts are permitted to spread energy over a *source surface*. Similarly, receivers are located on a *receiver surface*. Assuming that the presumed point source is at location $\mathbf{x}_s$, a simple (though certainluy not the only) choice for the penalty operator A is then multiplication by the distance $|\mathbf{x} - \mathbf{x}_s|$ to the physical source location:

$$(A\mathbf{f})(\mathbf{x}, t) = |\mathbf{x} - \mathbf{x}_s|\mathbf{f}(\mathbf{x}, t) \tag{5}$$

I shall use this choice of penalty operator whenever a specific choice is necessary in the development of the theory below.

This paper presents a numerically efficient approach to solving the *source sub-*

problem of problem 4:

$$\text{given } \mathbf{c},\ \text{choose surface source } \mathbf{f} \text{ to minimize } \|PL[\mathbf{c}]^{-1}\mathbf{f} - d\|^2 + \alpha\|A\mathbf{f}\|^2 \quad (6)$$

Solution of this subproblem is an essential component of *variable projection* algorithms for solution of the nonlinear inverse problem 4. Variable projection is not merely a convenient choice of algorithm for this purpose: it is in some sense essential, see for example Symes et al. (2020). It replaces the nonlinear least squares problem 4 with a *reduced* problem, to be solved iteratively. Each iteration involves solution of the subproblem 6. Therefore efficient solution of the subproblem is essential to efficient solution of the nonlinear problem via variable projection.

The modeling operator $PL[\mathbf{c}]^{-1}$ and the penalty operator A defined in 5 are linear, so the source subproblem is a linear least squares problem. Under some additional assumptions to be described below, I shall show how to construct an accurate approximate solution operator for problem 6. This approximate solution operator may be used to accelerate ("precondition") Krylov space methods for the solution of the surface source subproblem 6. I will fully describe a preconditioner for a special case of the source subproblem 6, in which $\mathbf{u}$ is an acoustic field, $L[\mathbf{c}]$ is the wave operator of linear acoustodynamics, and the source and receiver surfaces are horizontal planes. Numerical examples in this setting suggest the effectiveness of this acceleration.

I will use two 2D numerical models throughout to illustrate the theory. In both, horizontal lines serve as source and receiver surfaces. The first is a "horizontal crosswell" or slab configuration with an acoustic lens positioned between a deep source and a shallower line of receivers, resulting in markedly triplicated arrivals. The goal in this first example is to construct a surface source that explains the data in a homogeneous medium (that is, inversion in a wrong velocity, emulating the early iterations of FWI based on extended modeling). The second is a layered model in which velocity increases with depth, resulting the formation of diving waves. This configuration simulates an ocean-bottom node and a line of near-surface sources: the roles of source and receiver are switched for computational convenience. In this second example, the diving wave arrivals are isolated (by an appropriate mute operator) and a source constructed that explains them alone.

Since the constructions described here involve a significant number of components and ideas, I begin the paper with an overview, mapping out the key steps and their relation to other work. The next section defines the modeling operator $PL[\mathbf{c}]^{-1}$ and important specializations (pressure vs. normal velocity sources and data). It also introduces the two 2D examples mentioned above. The following section constructs an approximate inverse of the modeling operator by time reversal (as suggested by work in photoacoustic tomography), and illustrates its efficacy via the two examples. This construction requires extraction of velocity data, or equivalently a surface source, from pressure data. The subsequent sections describe this pressure-to-source operator, express the approximate inverse as the modeling operator adjoint in weighted norms (thus establishing that the modeling operator is *approximately unitary* in the sense

of these norms), explain how to use this construction to precondition Conjugate Gradient iteration, and organize the preconditioning computation so as to involve only one extra and relatively inexpensive wave propagation calculation. I use the 2D examples to illustrate each of these developments. The paper ends with a brief discussion-and-conclusion section, reviewing what has been accomplished and listing a few of the many questions left open.

OVERVIEW

The preconditioner construction is partly inspired by the time reversal method in photoacoustic tomography (Stefanov and Uhlmann, 2009; Hristova, 2009). This problem clearly has strong similarities to, but also differences from, the problem studied here.

A simplified mathematical translation of this medical imaging task is to infer the initial excess pressure distribution over a fluid-containing region at time $t = 0$ from measurements of the pressure on a surface enclosing the fluid over a time interval $0 \leq t \leq t_{\max}$. The time reversal method presumes that the pressure field has returned to equilibrium (zero excess pressure), or close to it, in the fluid-containing region at the final time $t = t_{\max}$ Then the field can be (at least approximately) viewed as the backwards-in-time initial boundary value problem with zero final conditions at $t = t_{\max}$, and boundary values given by the measurements. Evolving the field backwards in time backwards to $t = 0$ thus solves the problem. Except in special circumstances, the pressure field never actually vanishes at finite time, so the solution is approximate.

The seismic surface source extension proplem 6 differs in several obvious ways from the photoacoustic setting. The measurement or receiver surface does not surround the region of wave propagation. It is not the initial pressure time-slice at $t = 0$ that is to be determined, but a time-extended source $\mathbf{f}$ confined to a surface. The penalty operator A has no analogue in the basic photoacoustic problem description. Finally, once these obstacles are overcome, using the approximate solution operator to accelerate Krylov iteration for solution of the optimization problem 6 requires that the operator be identified as the adjoint of the modeling operator with respect to suitable inner products in its domain and range. The next few paragraphs sketch resolutions of each of these issues.

First, reverse-time propagation can be localized via ray theory, within high-frequency asymptotic approximation. This step requires some assumptions about the ray fields: all rays responsible for significant energy in the receiver data must arrive from the source surface, and must cross the source and receiver surfaces transversally, that is, making non-zero angles. Also, the rays must approach source and receiver surfaces from one side or the other ("the inside"), so that locally the surfaces can be treated as boundaries of propagation domains. Specifically, rays must emanate from the source surface towards the inside ("incoming" rays), and arrive at the receiver surface from the inside ("outgoing" rays). With these assumptions, reverse-time propagation of

the receiver data closely approximates the acoustic fields near the source surface. Next observe that for a causal field with a surface pressure source (with a continuous pressure field across the surface), the source is proportional to the jump in the (particle) velocity field. Moreover, to leading order in frequency, the velocity field switches sign at the surface, so the jump is just twice the sampled value on the surface. Thus reverse-time propagation and reading off the velocity field on the source surface yields a source that reproduces the pressure data, within an asymptotically small error.

This is the essence of the approximate solution of the problem 6 for penalty weight $\alpha = 0$. To see how Krylov iteration might be accelerated, note that time-reverse propagation of the receiver pressure values may be represented by a time-reverse source propagation, with the source constructed from the velocity field at the receiver surface. Moreover, the reverse-time source-to-pressure propagation is the transpose (adjoint) of the forward-time source-to-pressure propagation - this is a very simple version of the adjoint state construction (Plessix, 2006). So the approximate inverse may be described as: conversion of pressure to source at the receiver surface, followed by the adjoint of the modeling operator, followed by the conversion of pressure to source at the source surface. This sequence precisely describes the adjoint of the modeling operator with respect to weighted norms in the spaces of source and receiver data, with the weight operators being the pressure-to-source operators. That this construction results in an approximate inverse means that the modeling operator is approximately unitary with respect to these weighted norms, which in turn implies that a properly constructed preconditioned conjugate gradient algorithm should converge rapidly.

FInally, the $\alpha = 0$ case is not sufficient: the penalty operator A is an essential component of the nonlinear inverse propblem 4. As it turns out, A commutes with the other operators involved - approximately, but that is enough. Therefore the effect of A can be compensated with an easily-computed factor, whence the preconditioned acceleration extended to the case $\alpha > 0$.

This pressure-to-source map is closely related to the "hyperbolic Dirichlet-to-Neumann" operator that plays a prominent role in photoacoustic tomography and other wave inverse problems (Rachele, 2000; Stefanov and Uhlmann, 2005). Hou and Symes (2016b) demonstrated a very similar preconditioner for Least Squares Migration, also for its subsurface offset extension (Hou and Symes, 2016a), motivated by ten Kroode (2012). These constructions also involve the Dirichlet-to-Neumann operator. This concept also turns up in hidden form in the work of Yu Zhang and collaborators on true amplitude migration (Zhang et al., 2014; Tang et al., 2013; Xu et al., 2012, 2011; Zhang and Sun, 2009).

The discussion in this paper is formal and incomplete, in the sense that some important mathematical underpinnings are only sketched. I will treat the modeling operator $PL[\mathbf{c}]^{-1}$ as if it mapped square integrable surface sources to square integrable sampled data. This is not true in full generality: while the surface source problem has distribution solutions, they are not generally square integrable (finite acoustic field energy). Even if the solutions have finite energy, they do not in general have well-defined restrictions to lower-dimensional sets. In other words, the action of the

sampling operator P on the receiver surface is not well-defined for arbitrary finite-energy acoustic fields. Thus the modeling operator envisioned above is not be well-defined, strictly speaking.

This phenomenon is related to the ill-posedness of wave equations as evolution equations in spatial variables, an observation attributed to Hadamard (see Courant and Hilbert (1962), Chapter 6, section 17). A number of authors have described precise forms of the ray conditions described above, and shown how these conditions lead to the desired behaviour of the modeling operator, that is, mapping of finite energy sources to finite energy data, or equivalent properties Payne (1975); Symes and Payne (1983); Lasiecka (1986); Lasiecka et al. (1986); Lasiecka and Trigianni (1989); Bao and Symes (1991). Elaboration of these mathematical details is beyond the scope of this paper, which aims instead to explore the algorithmic consequences of the mathematical structure implied by the nongrazing hypothesis.

OPERATORS

For acoustic wave physics, the coefficient vector is $\mathbf{c} = (\kappa, \rho)^{\mathbf{T}}$, with components bulk modulus κ and density ρ, and the state vector $\mathbf{u} = (p, \mathbf{v})^T$ consists of pressure p (a scalar space-time field) and particle velocity $\mathbf{v}$ (a vector space-time field). The wave operator $L[\mathbf{c}]$ is:

$$L[\mathbf{c}]\mathbf{u} = \begin{pmatrix} \frac{1}{\kappa}\frac{\partial p}{\partial t} + \nabla \cdot \mathbf{v}, \\ \rho\frac{\partial \mathbf{v}}{\partial t} + \nabla p. \end{pmatrix} \tag{7}$$

That is,

$$L[\mathbf{c}] = \begin{pmatrix} \frac{1}{\kappa}\frac{\partial}{\partial t} & \nabla \cdot \\ \nabla & \rho\frac{\partial}{\partial t} \end{pmatrix} \tag{8}$$

$L[\mathbf{c}]$ has a well-defined inverse if it is restricted to either causal or anti-causal vector wavefields.

Since all of the operators in the discussion that follows depend on the coefficient vector $\mathbf{c}$, I will suppress it from the notation, for example, $L = L[\mathbf{c}]$.

Most of what follows is valid for any space dimension $n > 0$. I will describe the theory for $n = 3$, write $\mathbf{x} = (x, y, z)^T$ for the spatial coordinate vector, and similarly for the particle velocity $\mathbf{v} = (v_x, v_y, v_z)$. For computational convenience, the examples are two-dimensional.

The surface source extension replaces point sources on or near a surface Σ_s in $\mathbf{R}^3$ with source functions confined to the surface . The surface should be supplied with a choice of unit normal vector field $\mathbf{n}_s$. Since the surface separates space into two non-overlapping parts, at least locally, designate the part into which the normal vector points as the "outside", so that $\mathbf{n}_s$ is the outward normal.

For acoustic modeling, surface sources are combinations of constitutive law defects and loads normal to the surface, localized on Σ_s. That is, right-hand sides in the

system $L\mathbf{u} = \mathbf{f}$ take the form $\mathbf{f}(\mathbf{x}, t) = (h_s\delta_{\Sigma_s}, f_s\mathbf{n}_s\delta_{\Sigma_s})^T$ for scalar defect h_s and normal load f_s. With the choice L given in 8, the causal system $L\mathbf{u} = \mathbf{f}$ takes the form

$$\begin{aligned} \frac{1}{\kappa}\frac{\partial p}{\partial t} &= -\nabla\cdot\mathbf{v} + h_s\delta_{\Sigma_s}, \\ \rho\frac{\partial \mathbf{v}}{\partial t} &= -\nabla p + f_s\mathbf{n}_s\delta_{\Sigma_s}, \\ p &= 0 \text{ for } t \ll 0, \\ \mathbf{v} &= 0 \text{ for } t \ll 0. \end{aligned} \tag{9}$$

Remark: In system 9 and many similar systems to follow, I will use the shorthand such as

$$p = 0 \text{ for } t \ll 0$$

to mean that p is *causal*, that is,

$$\text{For some } T \in \mathbf{R}, p(\cdot, t) = 0 \text{ for all } t < T.$$

Similarly,

$$p = 0 \text{ for } t \gg 0$$

signifies that p is anti-causal.

Extended forward modeling consists in solving 9 and sampling the solution components at a receiver surface Σ_r with ("outward") unit normal field $\mathbf{n}_r$. P_s and P_r are the sampling operators on Σ_s and Σ_r respectively. In practice, sampling necessarily occurs at a discrete array of points (trace locations), and over a zone of finite extent. In this theoretical discussion, I will neglect the finite sample rate, and regard the data, for example $P_r p$, as continuously sampled. The output samples are necessarily muted, that is, non-zero only over a space-time domain of finite extent. This mute, and any tapering applied to the data traces, are regarded as part of the sampling operators P_s, P_r.

The vector modeling operator $\mathcal{S}$ relates the source amplitudes h_s, f_s on Σ_s to the sampled pressure and normal velocity p, $\mathbf{v}\cdot\mathbf{n}_r$ for the solution $(p, \mathbf{v})$ of the systems 9 by

$$\mathcal{S}(h_s, f_s)^T = (P_r p, P_r(\mathbf{v}\cdot\mathbf{n}_r))^T, \tag{10}$$

Denote by $\Pi_i, i = 0, 1$ the projection on the first,respectively second, component of a vector in $\mathbf{R}^2$. The forward modeling operator from pressure source to pressure trace is

$$S = \Pi_0\mathcal{S}\Pi_0^T \tag{11}$$

With these conventions, we can write the version of the source subproblem 6

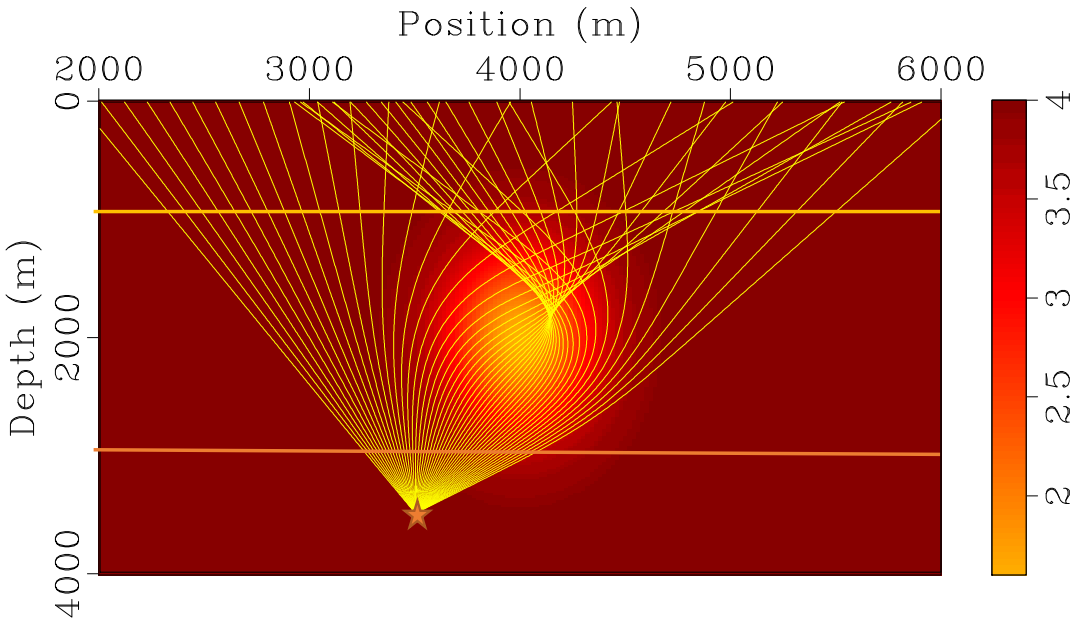

Figure 1: Bulk modulus with acoustic lens. Color scale unit is GPa. Orange horizontal line is source surface at depth $z_s = 3000$ m, yellow horizontal line is receiver surface at depth $z_r = 1000$ m. Point source location for data generation at $(3500, 3500)$ m indicated with star. Overlain with rays from point source to receiver surface.

studied in this paper as: given a pressure gather d on Σ_r,

$$\text{find } h_s \text{ to minimize } \|Sh_s - d\|^2 + \alpha^2 \|Ah_s\|^2. \tag{12}$$

The two examples mentioned in the introduction illustrate the setting just described. The first example (Figure 1) embeds an acoustic (low-velocity) lens between a source surface $\Sigma_s = \{z = z_s = 3000 \text{ m}\}$ (orange horizontal line) m and a receiver surface $\Sigma_r = \{z = z_r = 1000 \text{ m}\}$ (yellow horizontal line). The data to be used in this example results from a point source at $(3500, 3500)$ m (orange star). I have overlain the rays connecting this source point with the data portion of the receiver surface: evidently all of the rays involved cross the source and receiver surfaces transversally. Also, regarding "inwards" as being "upwards" at the source surface, "downwards" at the receiver surface, it is clear that the data is incoming at the source surface, outgoing at the receiver surface.

Figure 2a shows the gather $P_r p_{\text{pt}}$, where p_{pt} is causal field generated by the point source at $(3500, 3500)$ m with a trapezoidal bandpass filter wavelet having significant energy between 1 and 12.5 Hz. The mute embedded in P_r limits trace positions to 2000 m $\leq x_r \leq$ 6000 m, and times to 1.2 s $\leq t \leq$ 3 s.

Figure 2b displays an extended (pressure) source h_s, in the form of traces in the spatial range 2000 m $\leq x_r \leq$ 6000 m and time range 0 s $\leq t \leq$ 2 s. The modeling

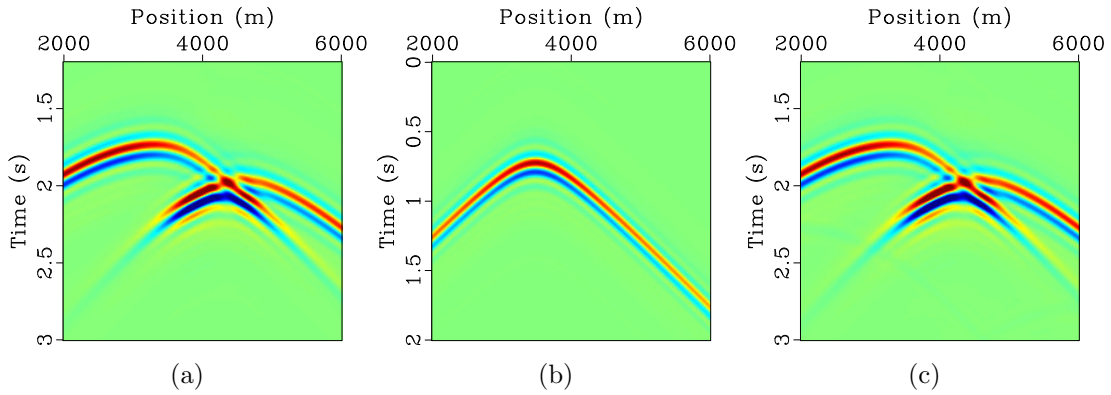

(a) (b) (c)

Figure 2: Data generated using configuration in Figure 1. (a) traces from point source at $(3500, 3500)$ with $[1, 2, 7.5, 12.5]$ Hz zero phase trapezoidal bandpass filter wavelet, delayed by 0.5 s. (b) Equivalent extended source on the source surface at depth $z_s = 3000$ m. (c) Gather generated by equivalent source shown in (b). Color scale is same for (a) and (c).

operator output Sh_s, obtained from the causal solution $(p, \mathbf{v})$ of 9 with this choice of h_s and $f_s = 0$, by application of the sampling operator P_r to p, is shown in Figure 2c.

Remark: The close resemblance between Figures 2a and 2c is not accidental - the extended source h_s shown in Figure 2b is constructed so that Sh_s (Figure 2c) closely approximates the point source gather $P_r p_{\text{pt}}$ (Figure 2a). This construction will be explained in the next section.

The second example is intended as a cartoon of long-offset node acquisition. It features a depth-dependent increasting velocity. Figure 3 shows bulk modulus field (once again, the density is constant and $= 1$ g/cm^3). The source and receiver surfaces are horizontal lines, as in the first example, at depths $z_s = 500$ m and $z_r = 100$ m respectively. A point source used to generate a data traces is positioned at $z_s = 500, x_s = 10000$ m. The source wavelet is the same bandpass filter as in the previous example.

A diving wave arrival is clearly visible in Figure 4a, which displays data traces over the position range $14000 \leq x_r \leq 20000$ m. The ray field connecting the point source to the receiver surface is plotted with the diving rays in blue, the rest in red. Note that at the source, the diving rays are incoming if the orientation is chosen with inwards = down, in contrast to the previous example, while they are outgoing at the receiver surface if it is oriented so that inwards = down also.

This geometry permits inversion of the diving wave data alone, which is isolated via a mute, depicted in Figure 4b. The mute includes time truncation at 6 s, and offsets between -10000 and 10000 m. The isolated diving wave (window between offsets 4000 and 10000) is shown in Figure 4c.

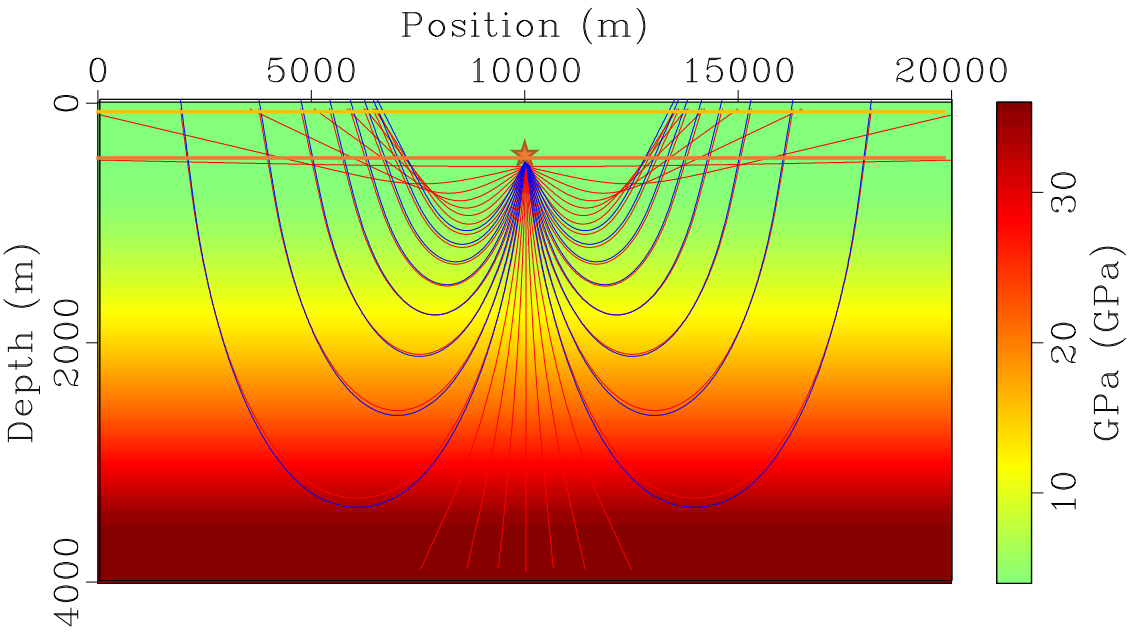

Figure 3: Bulk modulus generating diving waves. Color scale unit is GPa. Orange horizontal line is source surface at depth $z_s = 500$ m, yellow horizontal line is receiver surface at depth $z_r = 100$ m. Point source location for data generation at $(500, 10000)$ m indicated with star. Overlain with rays from point source to receiver surface.

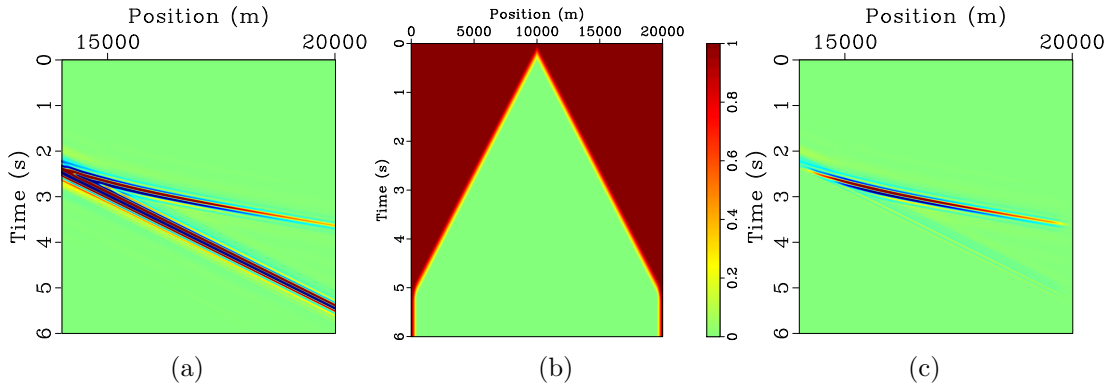

Figure 4: Data generated using configuration in Figure 3. (a) traces from point source at $(500, 10000)$ m with $[1, 2, 7.5, 12.5]$ Hz zero phase trapezoidal bandpass filter wavelet, delayed by 0.4 s. (b) Mute function, incorporated in the sampling operator P_r. (c) Diving wave gather. Color scale is same for (a) and (c).

TIME REVERSAL

Time reversal as found in the literature on photoacoustic tomography must be localized to apply to the surface source inversion problem, since there is no measurement surface surrounding the region of propagation. It must also be modified to produce a source, rather than a restriction of the pressure field. The assumption of incoming rays at the source surface and outgoing rays at the receiver surface makes both modifications possible.

The construction takes place in three stages: first, an acoustic field with high-frequency energy propagating along an incoming ray family is identified as the causal solution of an inhomogeneous boundary value problem *locally and on the inside*. The boundary value is simply the restriction of the acoustic field to the surface. Second, the same causal solution is identified as the causal solution of an acoustic problem with source, singular on the surface in the fashion of equation 9. The source amplitude is proportional to the velocity field sampled on the surface. Third, this identification is used twice, first to propagate the receiver data backwards in time as the solution of an anti-causal problem, the velocity field of which is sampled on the source surface; then the causal problem is solved with the source built from the velocity samples. This solution must be identical to the field generating the data, along the ray fields carrying all of the high-frequency energy. Therefore the reconstructed source is an approximate solution of the problem 6 for $\alpha = 0$.

Field localization

The first task is to view an acoustic field locally as a solution of a boundary value problem with prescribed pressure on the boundary of a domain, as is the case in the photoacoustic tomography configuration.

In this subsection $(p, \mathbf{v})$ is a solution of the homogeneous acoustic system

$$\begin{aligned} \frac{1}{\kappa}\frac{\partial p}{\partial t} &= -\nabla \cdot \mathbf{v}, \\ \rho\frac{\partial \mathbf{v}}{\partial t} &= -\nabla p, \end{aligned} \tag{13}$$

The source surface Σ is given a choice of unit normal field $\mathbf{n}$. Rays carrying high-frequency energy in $(p, \mathbf{v})$ pass through Σ, and intersect Σ only at times > 0. Also, the velocity vectors of all such rays have a negative $\mathbf{n}$ component where they cross Σ. Construct a time interval $[0, \tau]$ and a region in space Ω^+ containing Σ so that Σ forms part of the boundary $\partial\Omega^+$ of Ω^+, $\mathbf{n}$ is the outward unit normal to Ω^+ on Σ, and the energetic rays cross $\partial\Omega^+$ *only* at points of Σ in the time interval $[0, \tau]$ - that is, in time less than τ the rays do not reach other parts of $\partial\Omega^+$. Note that the rays are *incoming* to Ω^+ in the terminology introduced earlier. See Figure 5.

Consequent to this ray geometry, conclude that the field $(p, \mathbf{v})$ is asymptotically

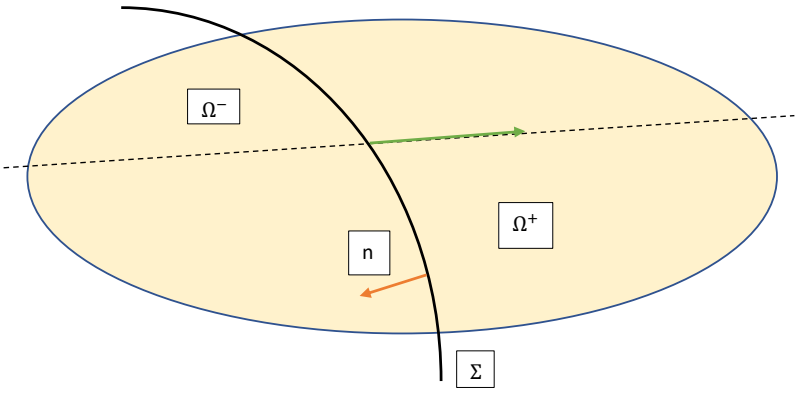

Figure 5: Localization near crossing points of rays. Σ is source surface. Dashed line is part of a ray carrying high frequency energy. Ray velocity vector has negative component in direction of unit normal $\mathbf{n}$ (outward, in chosen orientation). Ω^+ contains all ray segments for times $0 \leq t \leq \tau$ (green arrow). Rays intersect boundary $\partial\Omega^+$ only in Σ for this time range. Ω^- lies on outward side of Σ, which is part of its boundary. The domain Ω is the union of Ω^+ and Ω^-.

negligible both throughout Ω^+ at $t = 0$ and at all points of $\partial\Omega^+$ except for Σ, for $0 \leq t \leq \tau$. So $(p, \mathbf{v})$ differs negligibly from the solution of the boundary value problem

$$\begin{aligned}
\frac{1}{\kappa}\frac{\partial \tilde{p}}{\partial t} &= -\nabla \cdot \tilde{\mathbf{v}}, \\
\rho\frac{\partial \tilde{\mathbf{v}}}{\partial t} &= -\nabla \tilde{p}, && (14)\\
\tilde{p}(\mathbf{x}, t) &= p(\mathbf{x}, t) \text{ for } \mathbf{x} \in \Sigma, 0 \leq t \leq \tau, && (15)\\
\tilde{p}(\mathbf{x}, t) &= 0 \text{ for } \mathbf{x} \in \partial\Omega^+ \setminus \Sigma, 0 \leq t \leq \tau. && (16)
\end{aligned}$$

Source representation

The fields involved in the surface source extension are causal and source-generated, rather than solutions of boundary value problems such as the system 14. To transition to a source representation, begin by extending the domain Ω^+, lying on the incoming side of the surface Σ, to a full neighborhood Ω of sigma by adding a domain Ω^- on the outside (see Figure 5). Once again, construct Ω^- so that none of the rays carrying high-frequency energy cross the boundary of Ω^- except at Σ. Extend the field $(\tilde{p}, \tilde{\mathbf{v}})$ to the full neigborhood Ω by solving the system 14 with Ω^+ replaced by Ω^-. Thus the extended field is pieced together out of causal fields solving the boundary value problem on either side of the boudary, with *the same* boundary condition, that is, the trace of p on Σ. Thus the extended field is continuous in p. it is not however continuous in $\mathbf{v}$, as will be seen shortly. More precisely, the normal component $\mathbf{v} \cdot \mathbf{n}$

has a discontinuity, while the tangential components are continuous. The jump in $\mathbf{v}\cdot\mathbf{n}$ contributes a delta function to the gradient: as a field in the whole neigborhood Ω, $(\tilde{p},\tilde{\mathbf{v}})$ solves

$$\begin{aligned}
\frac{1}{\kappa}\frac{\partial\tilde{p}}{\partial t} &= [\mathbf{v}\cdot\mathbf{n}]_\Sigma\delta_\Sigma - \nabla\cdot\tilde{\mathbf{v}},\\
\rho\frac{\partial\tilde{\mathbf{v}}}{\partial t} &= -\nabla\tilde{p}, &(17)\\
\tilde{p}(\mathbf{x},t) &= 0 \text{ for } \mathbf{x}\in\partial\Omega, 0\le t\le\tau, &(18)\\
\tilde{p} &= 0 \text{ for } \mathbf{x}\in\Omega^+, t, &(19)\\
\tilde{\mathbf{v}} &= \mathbf{0} \text{ for } \mathbf{x}\in\Omega^+, t=0. &(20)
\end{aligned}$$

in which δ_Σ is the delta function on Σ. The square bracket denotes the jump in the quantity enclosed across Σ, from the outside to the inside. Since $\mathbf{n}$ points from the inside to the outside, this convention contributes another minus sign.

This representation is even better than it looks: since the ray families in $\Omega^\pm$ cross the boundary only at Σ within the prescribed time interval, the solution changes only by an asymptotically negligible amount in Ω for $0\le t\le\tau$ if the boundary condition is removed and the system is solved for all of space-time.

There is a downside, namely the apparent necessity of constructing the solution in Ω^- so that the jump of $\mathbf{v}\cdot\mathbf{n}$ may be computed. That is actually not necessary, however. This is best seen by analyzing a generic geometric optics component associated to the phase function ψ^+ in Ω^+ and its family of rays. The acoustic field is assembled by a sum (in the continuum, an integral) over such solutions. A particular summand looks like

$$a(\mathbf{x})e^{i\omega(t-\psi(\mathbf{x}))}. \tag{21}$$

for $\mathbf{x}\in\Omega^+$. The phase ψ solves the eikonal equation, the amplitude a the related transport equation. The restriction of p to Σ determines ψ (and a) restricted to Σ, essentially by Fourier synthesis. Since the eikonal equation is even in $\nabla\psi$, and ψ restricted to Σ determines the tangential derivatives of ψ, the normal component of $\nabla\psi$ is determined up to sign by the boundary values of p. The spatial component of a ray $X(t)$ associated to ψ solves the ordinary differential equation

$$\frac{dX}{dt} = \nabla\psi(X). \tag{22}$$

The normal component of this ray must be negative (in Ω^+) - this is the incoming condition, and guarantees that the ray does not intersect $t=0$ in Ω^+ near Σ, justifying the initial condition in 14. Similarly, the normal component must be positive in Ω^- near Σ. But both must have the same magnitude, since ψ solves the eikonal equation - so they are negatives of each other. For causal solutions such as $(\tilde{p},\tilde{\mathbf{v}})$, the Newton's

law equation in 14 is equivalent to

$$\tilde{\mathbf{v}}(\mathbf{x},t) = -\frac{1}{\rho}\int_{-\infty}^{t} ds \nabla\tilde{p}(\mathbf{x},s), \tag{23}$$

except at Σ. it follows that the normal components of $\tilde{\mathbf{v}}$ have limits at point of Σ that are opposite in sign: for $\mathbf{x} \in \Sigma$,

$$\lim_{\zeta\to 0}(\tilde{\mathbf{v}}(\mathbf{x},t)\cdot\mathbf{n}(\mathbf{x}+\zeta\mathbf{n})) = -\lim_{\zeta\to 0}(\tilde{\mathbf{v}}(\mathbf{x},t)\cdot\mathbf{n}(\mathbf{x}-\zeta\mathbf{n}))$$

whence

$$[\tilde{\mathbf{v}}\cdot\mathbf{n}] = 2\lim_{\zeta\to 0}(\tilde{\mathbf{v}}(\mathbf{x},t)\cdot\mathbf{n}(\mathbf{x}-\zeta\mathbf{n})) \approx 2\mathbf{v}\cdot\mathbf{n} \tag{24}$$

That is, at least over the short time interval $0 \le t \le \tau$, $(p,\mathbf{v})$ is asymptotically approximated in Ω^+ by $(\tilde{p},\tilde{\mathbf{v}})$, which solves

$$\begin{aligned}
\frac{1}{\kappa}\frac{\partial\tilde{p}}{\partial t} &= f\delta_\Sigma - \nabla\cdot\tilde{\mathbf{v}}, \\
\rho\frac{\partial\tilde{\mathbf{v}}}{\partial t} &= -\nabla\tilde{p}, && (25)\\
\tilde{p} &= 0 \text{ for } \mathbf{x}\in\Omega, t = 0, && (26)\\
\tilde{\mathbf{v}} &= \mathbf{0} \text{ for } \mathbf{x}\in\Omega, t = 0. && (27)
\end{aligned}$$

with $f = 2\mathbf{v}\cdot\mathbf{n}$ on Σ.

This result appears limited by the short time assumption (on τ) and the corresponding spatial localization to Ω^+. However neither of these apparent limitations is real. The short time assumption may be relaxed by windowing the fields to short time windows then adding up the results. The approximating fields $(\tilde{p},\tilde{\mathbf{v}})$ are themselves approximated by ray theory solutions. The assumptions on rays crossing source and receiver surfaces are global, and extend the approximation 34 globally. Thus the last two conditions may be replaced by the basic causality condition

$$\begin{aligned}
\ldots &= \ldots && (28)\\
\tilde{p} &= 0 \text{ for } t \ll 0, && (29)\\
\tilde{\mathbf{v}} &= \mathbf{0} \text{ for } t \ll 0. && (30)
\end{aligned}$$

The effect of this change on the receiver surface traces of $\tilde{p}$ and $\tilde{\mathbf{v}}$ is negligible.

An example has already appeared in Figure 2b. In this example, the field $(p,\mathbf{v})$ is the point source solution with the point source depicted in Figure 1, located at $(3500, 3500)$ m. The role of Σ is played by the source surface $z = z_s = 3000$ m, and near this surface the field solves the source-free system 17. The "inside" in this example is the region $z > z_s$, and the outward unit normal is therefore $\mathbf{n} = (0,0,-1)$. Thus $(p,\mathbf{v})$ should be asymptotically close to the solution $(\tilde{p},\tilde{\mathbf{v}})$ of the system 34 in the region $z < z_s$, at least at locations connected by the ray field shown in Figure

?? to the source surface, provided that the source amplitude f is chosen $= -2v_z$ on $\Sigma = \{z = z_s\}$. Figure 2b displays exactly this f, and 2c the traces of $\tilde{p}$ on the receiver surface $z = z_r = 1000$ m, which satisfies the ray condition. The extremely close match between Figures 2a (traces of p) and 2c is consistent with the conclusion reached here.

Approximate Inversion

The time-reversal construction can now be translated into the context of seismic surface source inversion. Assume that $(p, \mathbf{v})$ is a solution of the free-space acoustic system 17, with high-frequency energy carried by a ray family that satisfies the criteria described earlier: incoming at the source surface Σ_s with normal field $\mathbf{n}_s$, outging at the receiver surface Σ_r with normal field $\mathbf{n}_r$, and every ray crossing Σ_r meets Σ_s. The goal of this subsection is to describe a procedure that constructs a source field h_s on Σ_s so that $Sh_s \approx P_r p$, thus approximately inverting the modeling operator S.

The sampled fields $(P_r p, P_r \mathbf{v})$ on Σ_r is negligible for large t. Due the outgoing assumption, $(p, \mathbf{v})$ are negligible for large t near Σ_r. The integrated Newton's law 23 acquires a minus sign if the integration from $-\infty$ to t is replaced by integration from t to ∞. Apply the construction of the last subsection in reverse time, to conclude that $(p, \mathbf{v})$ is approximated by $(\tilde{p}, \tilde{\mathbf{v}})$, where the latter solves the time-reversed problem

$$\begin{aligned}
\frac{1}{\kappa}\frac{\partial \tilde{p}}{\partial t} &= h_r \delta_{\Sigma_r} - \nabla \cdot \tilde{\mathbf{v}}, \\
\rho \frac{\partial \tilde{\mathbf{v}}}{\partial t} &= -\nabla \tilde{p}, && (31) \\
\tilde{p} &= 0 \text{ for } t \gg 0, && (32) \\
\tilde{\mathbf{v}} &= \mathbf{0} \text{ for } t \gg 0. && (33)
\end{aligned}$$

with $h_r = -2P_r(\mathbf{v} \cdot \mathbf{n}_r)$.

By construction, high-frequency energy in $(\tilde{p}, \tilde{\mathbf{v}})$ is carried by the same ray family as for $(p, \mathbf{v})$. Every ray passes over Σ_s and is incoming there. Since $(p, \mathbf{v})$ vanishes for $t \ll 0$ near Σ_s, $(\tilde{p}, \tilde{\mathbf{v}})$ is negligible there, So the construction detailed in the last two sections is applicable again, and $(\tilde{p}, \tilde{\mathbf{v}})$ is approximated by the solution of

$$\begin{aligned}
\frac{1}{\kappa}\frac{\partial \hat{p}}{\partial t} &= h_s \delta_{\Sigma_s} - \nabla \cdot \hat{\mathbf{v}}, \\
\rho \frac{\partial \hat{\mathbf{v}}}{\partial t} &= -\nabla \hat{p}, && (34) \\
\hat{p} &= 0 \text{ for } t \ll 0, && (35) \\
\hat{\mathbf{v}} &= \mathbf{0} \text{ for } t \ll 0. && (36)
\end{aligned}$$

with $h_s = 2P_s(\tilde{\mathbf{v}} \cdot \mathbf{n}_r) \approx 2P_s(\mathbf{v} \cdot \mathbf{n}_r)$.

Summary

The surface source version of the time reversal construction involves three steps: given pressure data $P_r p$ on the receiver surface Σ_r for a solution $(p, \mathbf{v})$ of the system 17 satisfying the ray conditions,

1. create a source h_r on Σ_r by multiplying the corresponding normal velocity trace by -2: $h_r = -2P_r(\mathbf{v} \cdot \mathbf{n}_r)$;
2. propagate h_r backwards in time by solving the system 31 for the acoustic field $(\tilde{p}, \tilde{\mathbf{v}})$;
3. create a source h_s on Σ_s by multiplying tne normal velocity trace of $(\tilde{p}, \tilde{\mathbf{v}})$ by 2: $h_s = 2P_s(\tilde{\mathbf{v}} \cdot \mathbf{n}_s)$.

Then $P_r p \approx S h_s$.

The surface source representaion part of the construction shows that under the assumed ray conditions, a solution of 17 is asymptotically the same near the receive surface Σ_r as the solution of the system 9 with a suitable source $\tilde{f}_s$ (and zero velocity source, $h_s = 0$. Therefore this construction also inverts the modeling operator S in the sense that $Sh_s \approx S\tilde{h}_s$ if $P_r p \approx S\tilde{h}_s$. That is, this construction produces an asymptotic rightt inverse of S: it does not necessily (approximately) recover the source that generates the data, but recovers some source that generates the data.

Example: Lens

The first example uses the acoustic lens model (Figure 1, with Σ_s = horizontal line at depth 3000 m, and Σ_r = horizontal line at depth 1000 m. The pressure data to be inverted is the sampling of the pressure field on Σ_r, generated by the point source shown in the figure, at $(3500, 3500)$ m (Figure 2a. However, I will invert this data in a homogeneous medium with $\kappa \equiv 4$ GPa. These choice illustrate two facts about surface source inversion and the approximate inversion based on time reversal. First, the success of the inversion demostrates the insensitivity of the time reversal method to ray multipathing (triplication), evident in the data (Figure 2a). Second, it is entirely possible to invert data in a material model other than the one in which it was produced (in the case of synthetic data, of course). This capability is critically important in the application of the approximate inversion in nonlinear inversion, where the early iterations involve solution of the source estimation problem 6 at (possibly very) wrong material models $\mathbf{c}$. Successful extension methods maintain data fit throughout the course of the inversion.

As noted earlier (and visible in Figure 1), the acoustic field in this example satisfies the ray conditions on which the time reversal construction is based: The rays are incoming at Σ_s, outgoing at Σ_r and all rays carrying significant energy at points of

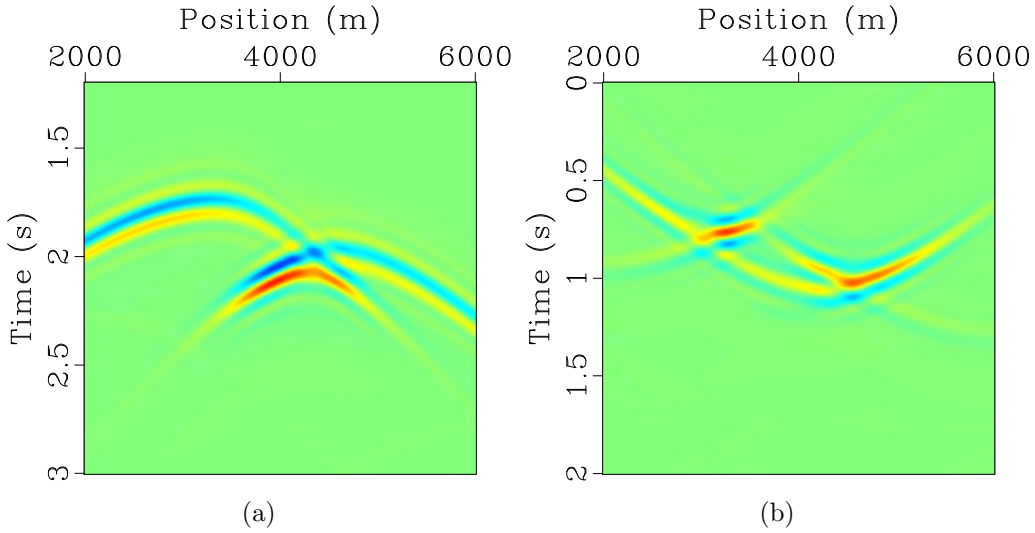

Figure 6: (a) Normal velocity data corresponding to pressure data in Figure 2c. (b) Source function resulting from time-reversal inversion of pressure data in Figure 2c. Propagation in homogeneous bulk modulus model (different from the model used to generate the data!). Plotted with same color scale as Figure 2b.

Σ_r pass over Σ_s. The outward unit normal at Σ_s is $\mathbf{n}_s = \mathbf{e}_z = (0, 1)$; at Σ_r, it's $\mathbf{n}_r = -\mathbf{e}_z = (0, -1)$. So the source on the receiver surface Σ_r, input to reverse time propagation (system 31, generating the fields $(\tilde{p}, \tilde{\mathbf{v}})$) is $h_r = 2P_r v_z$ (the field $P_r v_z$ is depicted in Figure 6a). After reverse time propagation , the approximate inversion $\tilde{h}_s = 2P_s\tilde{v}_z$ is shown in Figure **??**. It differs considerably from the source field used to generate the data (Figure 2b, however when used as the source in forward modeling (system 34) *with the same material parameters used in the inversion*, it generates a pressure gather on Σ_r (Figure 7a) very closely approximating the input gather (Figure 2c). The difference is plotted on the same color scale in Figure 7b.

Example: Diving Wave

The second example is based on the diving wave model (Figure 3). In this example, unlike the previous one, the source and receiver surfaces do not bound the propagating region, even in the vertical direction. Thus this exercise differs even more than the first from time reversal in photoacoustic tomography. Inspection of the blue part of the ray field in Figure 3 reveals that the rays are incoming at the source surface, and outgoing at the receiver surface, if the outward normal is chosen as $-\mathbf{e}_z$. The mute shown in Figure 4b eliminates the rest of the ray field. What remains satisfies the condition that every ray passing the receiver surface originates in the source surface.

In this example, the inversion is performed with the same model as used to generate the data. Note that sufficiently small changes in the model would result in

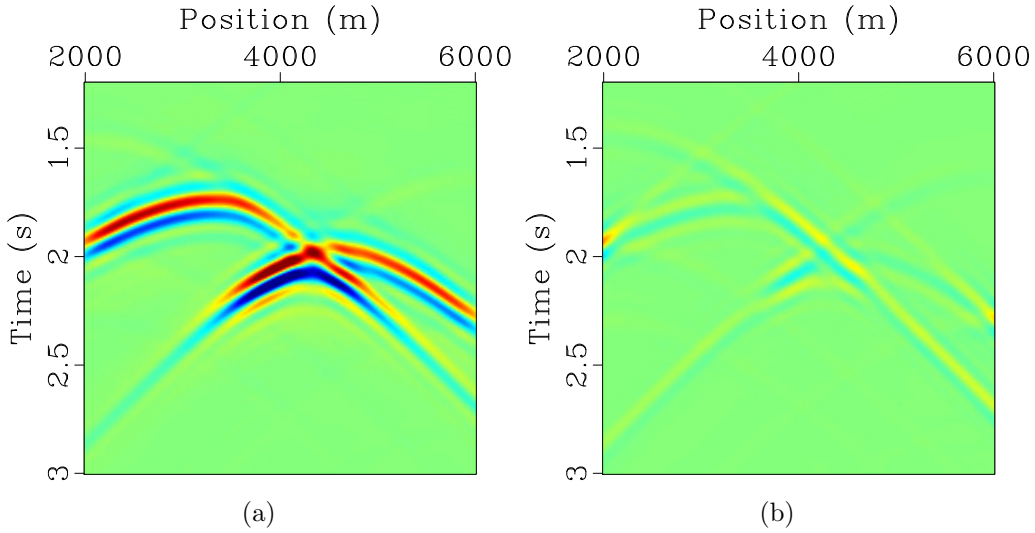

Figure 7: (a) Resimulated data: pressure gather generated from inverted source (Figure 6b, using same homogeneous bulk modulus as used in inversion. (b) Difference between data depicted in Figure 7a and in Figure 2c. Both (a) and (b) plotted with same color scale as Figure 2c.

similar ray configurations, so time reversal inversion could proceed as is shown here. However sufficiently large changes in the bulk modulus model could result in fundamental changes in the ray field: for instance, change to a homogenous model would completely eliminate the diving rays and the corresponding data component, thus making an inversion of the type presented here impossible.

The inversion proceeds otherwise as before. The source $h_r = -2P_r v_z$ on Σ_r is built from the normal component of velocity, shown in Figure 8a. Reverse time propagation to create the fields $(\tilde{p}, \tilde{\mathbf{v}})$, extraction of the normal component of velocity (note the sign difference with the previous example!) and scaling by the factor 2 produces the inverted source shown in Figure 8b. Forward propagation yields the pressure gather shown in Figure 9a, which closely matches the original diving wave pressure data (Figure 4c). The difference is displayed on the same color scale in Figure 9b.

PRESSURE-TO-SOURCE

Since the system 9 has a unique solution by standard theory (Lax, 2006), the source vector field (h_s, f_s) determines the acoustic field $(p^{\pm}, \mathbf{v}^{\pm})$ in space time, and in particular the limits from the right at $z = z_s$, $P_s p^{\pm}$ and $P_s v_z^{\pm}$. This relation is not invertible: it is not possible to prescribe both pressure and normal velocity on a surface such as $z = z_s$. So the columns of the matrix operator $\mathcal{S}^{\pm}_{z_s,z_r}$ must satisfy a linear relation. In this section I will explain this relation; it involves the *pressure-to-source* map. This operator also turns out to be the principal component of a preconditioning strat-

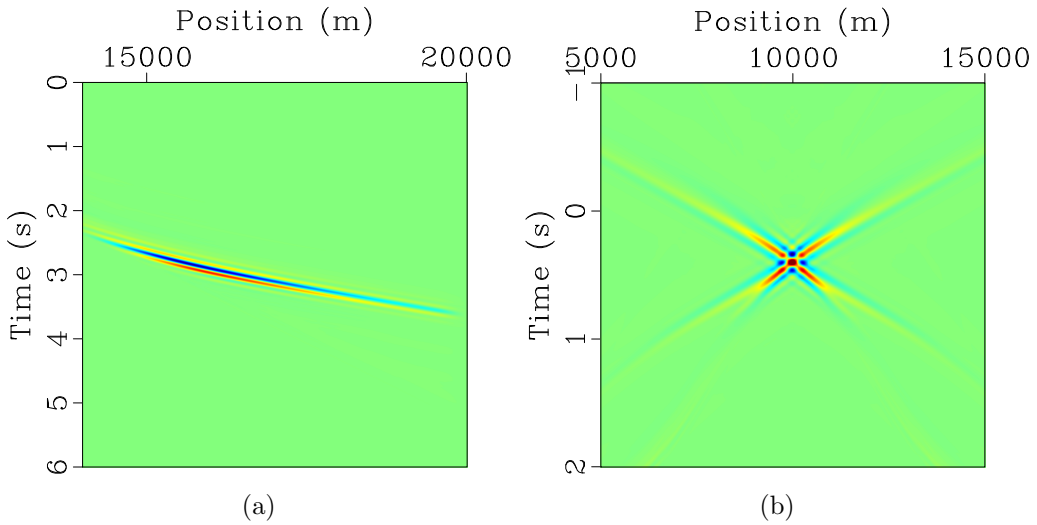

Figure 8: (a) Normal velocity data corresponding to pressure data in Figure 4c. (b) Source function resulting from time-reversal inversion of pressure data in Figure 4c. Propagation in same model (Figure 3) as used to generate the data.

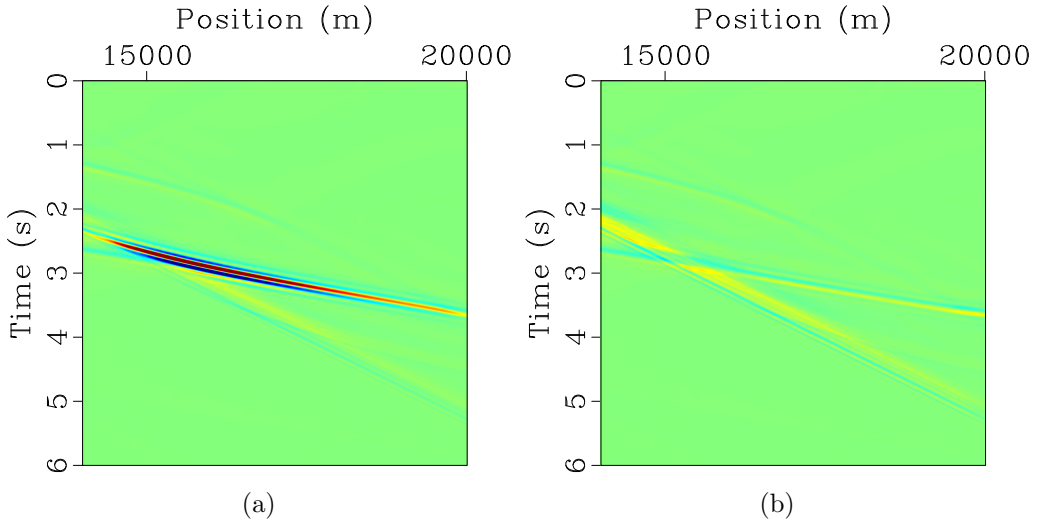

Figure 9: (a) Resimulated data: pressure gather generated from inverted source (Figure **??**, using same bulk modulus (Figure 3) as used in data generation and inversion. (b) Difference between data depicted in Figure 9a and in Figure 4c. Both (a) and (b) plotted with same color scale as Figure 4c.

egy for iterative solution of the optimization problem 6, so I will devote some effort to its proper definition. It is closely related to the Dirichlet-to-Neumann operator mentioned in the introduction.

While it is not possible to prescribe both pressure and velocity on $z = z_s$ in solutions of 9, it is possible to prescribe pressure only, for instance: if the function ϕ on the surface $z = z_s$ satisfies suitable conditions, for example the downgoing constraint mentioned earlier, a unique solution exists for the acoustic system in both half-spaces $\pm z > z_s$:

$$\begin{aligned} \frac{1}{\kappa}\frac{\partial p_\pm}{\partial t} &= -\nabla\cdot\mathbf{v}_\pm, \\ \rho\frac{\partial \mathbf{v}_\pm}{\partial t} &= -\nabla p_\pm, \\ p_\pm &= 0, \text{ for } t \ll 0, \\ \mathbf{v}_\pm &= 0 \text{ for } t \ll 0, \\ \lim_{z\to z_s^\pm} p_\pm(x,y,t,z) &= \phi(x,y,t). \end{aligned} \tag{37}$$

Note that the subscript $\pm$ here refers to the sign of $z - z_s$, as opposed to the superscript $\pm$, which refers to the sign of t throughout this paper.

From the boundary condition (last equation in 37), one sees that the pressures $p_\pm$ in the two half-spaces have the same limit at the boundary $z = z_s$. Stick the two half-space solutions together to form an acoustic field $(p^+, \mathbf{v}^+)$ in all of space-time, that is,

$$p^+(x,y,z,t) = \begin{cases} p_+(x,y,z,t) \text{ if } z > 0, \\ p_-(x,y,z,t) \text{ if } z < 0, \end{cases} \tag{38}$$

and a similar definition for $\mathbf{v}^+$. Then p^+ is continuous across $z = z_s$, and the boundary condition in system 37 may be written as $P_s p^+ = \phi$.

The same construction can be carried out in the anti-causal sense, with anti-causal half-space solutions glued together to form a full-space distribution solution $(p^-, \mathbf{v}^-)$, with the property that p^- is continuous across $z = z_s$ and $P_s p^- = \phi$.

The reader may object that the notation $(p^\pm, \mathbf{v}^\pm)$ is already in use, for the solution of 9. This objection is valid. However, *in the sense of distributions*, $(p^\pm, \mathbf{v}^\pm)$ as defined in display 38, is *exactly* the causal solution of 9 for the choice $h_s = -[v_z^\pm]|_{z=z_s}$, $f_s = 0$, as follows from a simple integration-by-parts calculation. So the notation is consistent!

The negative jump $-[v_z^\pm]|_{z=z_s}$ is thus a function of ϕ. Define the *pressure-to-source* operator $\Lambda_{z_s}^\pm$ by

$$\Lambda_{z_s}^\pm \phi = -[v_z^\pm]|_{z=z_s} \tag{39}$$

The conclusion: if $h_s = \Lambda_{z_s}^\pm \phi$ and $f_s = 0$ in the system 9, then $\phi = P_s p^\pm$.

Otherwise put, $S_{z_s,z_s}^\pm \Lambda_{z_s}^\pm \phi = \phi$, so $\Lambda_{z_s}^\pm$ is inverse to $S_{z_s,z_s}^\pm$. The relation **??** implies

in turn that

$$(\Lambda_{z_s}^{\pm})^T = -\Lambda_{z_s}^{\mp} \tag{40}$$

There is also a *velocity-to-source* operator. For the solution $(p^{\pm}, \mathbf{v}^{\pm})$ of system 9 with $h_s = 0$, the normal component of velocity, $v_z^{\pm}$, is continuous across $z = z_s$, and the velocity source (vertical load) $f_s = -[p^{\pm}]_{z=z_s}$. I will not name the velocity-to-source operator, as it does not appear explicitly in the developments to follow. As will be seen, it is essentially the inverse of the pressure-to-source operator.

The quadratic form defined by $\Lambda_{z_s}^{\pm}$ has fundamental physical significance. Define the total acoustic energy $E^{\pm}(t)$ of the field $(p^{\pm}, \mathbf{v}^{\pm})$, at time t by

$$E^{\pm}(t) = \frac{1}{2}\int d\mathbf{x}\left(\frac{(p^{\pm})^2}{\kappa} + \rho|\mathbf{v}^{\pm}|^2\right)(\mathbf{x}, t). \tag{41}$$

Then

$$\pm \lim_{\pm t\to\infty} E^{\pm}(t) = \langle P_s p^{\pm}, (\Lambda_{z_s}^{\pm} P_s p^{\pm})\rangle_{L^2(z=z_s)}. \tag{42}$$

That is, the value of the quadratic form defined by $\Lambda_{z_s}^{\pm}$, evaluated at the pressure trace on $z = z_s$, gives the total energy transferred from the source to the acoustic field over time. Since E is itself a positive definite quadratic form in the acoustic field, it follows that $\pm\Lambda_{z_s}^{\pm}$ is positive semi-definite.

While $\Lambda_{z_s}^{\pm}$ is positive semi-definite, it is not symmetric. However, it is *approximately symmetric* in the high-frequency sense. This fact follows from a geometric optics analysis of the half-space solution. This leads to the identification of $\Lambda_{z_s}^{\pm}$ as a *pseudodifferential operator* of order zero on $z = z_s$, with principal symbol

$$\sigma_0(\Lambda_{z_s}^{\pm}) = \pm 2(\kappa(\mathbf{x})\rho(\mathbf{x}))^{1/2}\left(1 - \frac{\kappa(\mathbf{x})(\xi^2+\eta^2)}{\rho(\mathbf{x})\omega^2}\right)^{-1/2}. \tag{43}$$

Here ξ, η, and ω are the dual Fourier variables to x, y, and t respectively. The downgoing assumptions means that for local planewave components of $P_s p$, the quantity inside the square root is positive. Thus $\Lambda_{z_s}^{\pm}$ has real principal symbol (in fact, the entire symbol is real) hence defines an asymptotically symmetric operator:

$$(\Lambda_{z_s}^{\pm})^T \approx \Lambda_{z_s}^{\pm}. \tag{44}$$

(For more on this, see Stefanov and Uhlmann (2005).) The analysis also reveals that the solution components not continuous at $z = z_s$ are odd there:

$$\lim_{z\to z_s^+} v_z^{\pm} \approx -\lim_{z\to z_s^-} v_z^{\pm} \tag{45}$$

for the solution of 9 with $f_s = 0$. Similarly,

$$\lim_{z\to z_s^+} p^{\pm} \approx -\lim_{z\to z_s^-} p^{\pm} \tag{46}$$

for the solution of 9 with $h_s = 0$. Here "$\approx$" means in the sense of high frequency asymptotics, that is, that the difference between the two sides is relatively smooth, hence small if the data is highly oscillatory. Therefore if $f_s = 0$ in system 9,

$$h_s = \Lambda^{\pm}_{z_s} P_s p^{\pm} = -[v_z^{\pm}]|_{z=z_s} \approx -2P_s v_z^{\pm} \tag{47}$$

Similarly, if $h_s = 0$ in system 9, then

$$f_s = -[p^{\pm}]|_{z=z_s} \approx -2P_s p^{\pm}. \tag{48}$$

Thus f_s determines approximately the boundary value of $p^{\pm}$, as a solution of the acoustic wave system in the half-space $z > z_s$. However, as repeated in equation 47, a solution with this boundary value is also the restriction to $z > z_s$ of a solution to 9 with $f_s = 0$ and $h_s = \Lambda^{\pm}_{z_s} P_s p^{\pm}$. Therefore if

$$h_s = -\frac{1}{2}\Lambda^{\pm}_{z_s} f_s, \tag{49}$$

then the pressure boundary value $P_s p^{\pm}$ is the same for the solutions of 9 for source vectors $(h_s, 0)$ and $(0, f_s)$. Since the pressure boundary values are the same, the solutions in $z > z_s$ are the same. In particular, since $z_r > z_s$ and $\mathcal{S}^{\pm}_{z_s,z_r}(h_s, f_s)^T = (P_r p^{\pm}, P_r v_z^{\pm})^T$, it follows that

$$\mathcal{S}^{\pm}_{z_s,z_r}\left(\frac{1}{2}\Lambda^{\pm}_{z_s} f_s, f_s\right)^T \approx 0. \tag{50}$$

Equation 50 states the relation between the columns of $\mathcal{S}^{\pm}_{z_s,z_r}$ mentioned in the introduction to this section.

UNITARITY

The next chapter in this story recognizes the relations in display **??** as asserting the approximate unitarity of $S^{+}_{z_s,z_r}$.

The matrix identity 50 implies a relation between S, V, and Λ of some interest in itself. After minor re-arrangement, the second row of reads

$$-\frac{1}{2}\Pi_1 \mathcal{S}^{\pm}_{z_s,z_r}\Pi_0^T \Lambda^{\pm}_{z_s} \approx V^{\pm}_{z_s,z_r}. \tag{51}$$

In these relations, the projection on the left picks out the vertical velocity component of a downgoing wavefield at $z = z_r$: that is,

$$-\frac{1}{2}\Pi_1 \mathcal{S}^{\pm}_{z_s,z_r}\Pi_0^T \Lambda^{\pm}_{z_s} P_s p^{+} = -\frac{1}{2} P_r v_z^{+},$$

where $(p^+, \mathbf{v}^+)$ solve the system 9 with $f_s = 0$ and $h_s = \Lambda^{\pm}_{z_s} P_s p^{+}$. On the other hand,

from relation 47,

$$P_r v_z^+ = -\frac{1}{2}\Lambda_{z_r}^+ P_r p^+$$

where

$$\begin{aligned} P_r p^+ &= \Pi_0 \mathcal{S}_{z_s,z_r}^+ \Pi_0^T \Lambda_{z_s}^+ P_s p^+ \\ &= S_{z_s,z_r}^+ \Lambda_{z_s}^+ P_s p^+ \end{aligned}$$

Therefore combining the last two equations with 51, obtain

$$\frac{1}{4}\Lambda_{z_r}^+ S_{z_s,z_r}^+ \Lambda_{z_s}^+ = V_{z_s,z_r}^+. \tag{52}$$

This is the promised relation.

As shown in the last section, $4(V_{z_s,z_r}^+)^T$ is approximately inverse to S_{z_s,z_r}^+. Therefore, transposing both sides of equation 52 and using **??**, obtain

$$4(V_{z_s,z_r}^+)^T S_{z_s,z_r}^+ = [(\Lambda_{z_s}^+)^T (S_{z_s,z_r}^+)^T (\Lambda_{z_r}^+)^T] S_{z_s,z_r}^+ \approx I. \tag{53}$$

The remarkable feature of the identity 53 is that it exhibits an approximate right inverse of S^+ as an adjoint with respect to a weighted inner product - or it would, if the operators (Λ^+) were symmetric positive definite. As noted earlier, these operators are only approximately symmetric, though they are positive semi-definite. That is not a great obstacle, however: symmetrizing them in the obvious way commits a negligible error, of the sort that this paper already neglects wholesale. That is,

$$[\frac{1}{2}((\Lambda_{z_s}^+)^T + \Lambda_{z_s}^+)(S_{z_s,z_r}^+)^T \frac{1}{2}((\Lambda_{z_r}^+)^T + \Lambda_{z_r}^+)] S_{z_s,z_r}^+ \approx I. \tag{54}$$

The symmetrized Λ operators are at least positive semi-definite, hence define (at least) semi-norms. Similar relations have been derived for other scattering operators, and have been used to accelerate iterative solutions of inverse scatering problems: Dafni and Symes (2018) review some of this literature.

ACCELERATED ITERATIVE INVERSION

For convenience, in this section write S in place of S_{z_s,z_r}^+. Also abbreviate the symmetrized Λ operators using notation suggesting weight operators in model and data spaces:

$$\begin{aligned} W_m^{-1} &= \frac{1}{2}((\Lambda_{z_s}^+)^T + \Lambda_{z_s}^+), \\ W_d &= \frac{1}{2}((\Lambda_{z_r}^+)^T + \Lambda_{z_r}^+). \end{aligned} \tag{55}$$

The identification of the symmetrized $\Lambda_{z_s}^+$ as the inverse of another operator W_m is formal, since the former operator is likely to have null (or nearly-null) vectors due to aperture-related amplitude loss. Since some version of W_m is essential in the formulation for effective preconditioning, I will derive a usable candidate to stand in for it below.

Adopting Hilbert norms defined by the operators W_m and W_d in its domain and range respectively, the adjoint of S is given by

$$S^\dagger = W_m^{-1} S^T W_d, \tag{56}$$

In this notation, the relation 54 takes the form

$$S^\dagger S \approx I. \tag{57}$$

That is to say, S is approximately unitary with respect to the weighted norms defined by W_m and W_d. Therefore a Krylov space method employing these norms will converge rapidly, at least for the well-determined components of the solution.

The most convenient arrangement the Conjugate Gradient (CG) algorithm taking advantage of the structure 56 is the *Preconditioned CG*. Allowing that the fit error will be measured by the data space norm, the least squares problem to be solved is not just $Sh \approx d$, but a regularized version:

$$\text{minimize}_h \|Sh - d\|_d^2 + \alpha^2 \|Ah\|_m^2 \tag{58}$$

Remark: recall that the modified data space norm $\|d\|_d^2 = \langle d, W_d d\rangle$ has physical meaning: for acoustics, it is proportional to the power transmitted to the fluid by the source.

The minimizer of the objective defined in equation 58 solves the normal equation

$$(S^\dagger S + \alpha^2 A^\dagger A)h = S^\dagger d \tag{59}$$

where the weighted adjoint $S^\dagger$ has already been defined in equation 56, and $A^\dagger$ is the adjoint of A in the weighted model space norm defined by W_m, namely

$$A^\dagger = W_m^{-1} A^T W_m. \tag{60}$$

Note that the normal operator appearing on the left-hand side of 59 is not an approximate identity, due to the presence of the regularization term: the spectrum increases in spread with increasing α, leading to slower convergence. Fortunately for the present setting, the operators W_m^{-1}, A, and W_m approximately commute (they are scalar *pseudodifferential*, once the difficulties with the definition of W_m, mentioned above, are taken care of). Scalar pseudodifferential operators approximately

commute, so $A^\dagger \approx A^T$. Therefore

$$S^\dagger S + \alpha^2 A^\dagger A \approx I + \alpha^2 A^T A \tag{61}$$

Recall that A is simply multiplication by the Euclidean distance to the physical source point $\mathbf{x}_s$: $Au(\mathbf{x}) = |\mathbf{x} - \mathbf{x}_s| u(\mathbf{x}), A^T A u(\mathbf{x}) = |\mathbf{x} - \mathbf{x}_s|^2 u(\mathbf{x})$. So the equation $(I + \alpha^2 A^T A)u = b$ is trivial to solve, and this is a key characteristic of a good preconditioner. However this observation must be combined with the weighted norm structure.

Rewrite the normal equation 59 as

$$W_m^{-1}(S^T W_d S + \alpha^2 A^T W_m A)h = W_m^{-1} S^T W_m d \tag{62}$$

Since W_m is self-adjoint and positive semidefinite, the common factor on both sides of 62 can be re-written as

$$Nh = (S^* S + \alpha^2 A^* A)h = S^* d \tag{63}$$

in which S^*, A^* are the adjoints with the original (Euclidean) inner product in the domains but the weighted inner product in data space:

$$S^* = S^T W_d, \tag{64}$$
$$A^* = A^T W_m. \tag{65}$$

Note the S^*S and A^*A are symmetric in the Euclidean sense, so equation 63 is a symmetric positive (semi-)definite linear system, just the sort of thing for which the The Preconditioned Conjugate Gradient ("PCG") algorithm was designed. PCG for solution of equation 63 with preconditioner M is usually written as Algorithm 1 (see for example Golub and van Loan (2012)):

Algorithm 1 Preconditioned Conjugate Gradient Algorithm, Standard Version

Choose $h_0 = 0$
$r_0 \leftarrow S^* d$
$p_0 \leftarrow M^{-1} r_0$
$g_0 \leftarrow p_0$
$q_0 \leftarrow N p_0$
$k \leftarrow 0$
repeat
  $\alpha_k \leftarrow \frac{\langle g_k, r_k \rangle}{\langle p_k, q_k \rangle}$
  $h_{k+1} \leftarrow h_k + \alpha_k p_k$
  $r_{k+1} \leftarrow r_k - \alpha_k q_k$
  $g_{k+1} \leftarrow M^{-1} r_{k+1}$
  $\beta_{k+1} \leftarrow \frac{\langle g_{k+1}, r_{k+1} \rangle}{\langle g_k, r_k \rangle}$
  $p_{k+1} \leftarrow g_{k+1} + \beta_{k+1} p_k$
  $q_{k+1} \leftarrow N p_{k+1}$
  $k \leftarrow k + 1$
until Error is sufficiently small, or max iteration count exceeded

The iteration converges rapidly if $M^{-1}N \approx I$. This is true if and only if the symmetrized operator $M^{-1/2} N M^{-1/2} \approx I$, which is in turn true if the eigenvalues of $M^{-1/2} N M^{-1/2}$ are close to 1 (actually works well is most of these eigenvalues are close to 1, and the rest are small - which is the case for the current problem).. Further, PCG is computationally effective is M is easy to invert.

From 61 and 62, it follows that

$$W_m^{-1}(S^T W_d S + \alpha^2 A^T W_m A) \approx I + \alpha^2 A^T A.$$

This observation suggests using $M = W_m(I + \alpha^2 A^T A)$. This choice is not symmetric, but since the operators on the right-hand side are scalar pseudodifferential hence commute, it is equivalent to use of

$$\begin{aligned} M &= (I + \alpha^2 A^T A)^{1/2} W_m (I + \alpha^2 A^T A)^{1/2}, \\ M^{-1} &= (I + \alpha^2 A^T A)^{-1/2} W_m^{-1} (I + \alpha^2 A^T A)^{-1/2}. \end{aligned} \tag{66}$$

With this choice, 61 implies that $M^{-1}N \approx I$, also M is symmetric. As already mentioned, powers of $I + \alpha^2 A^T A$ are trivial to compute, given the choice of A made here. We will examine fast algorithms for computing W_m^{-1} = the symmetrized pressure-to-source operator in the next section. Note that only M^{-1}, hence only W_m^{-1}, appears in Algorithm 1.

COMPUTING AND SYMMETRIZING Λ

Computations of $\Lambda^{\pm}_{z_s}$ and its transpose are clearly critical steps in an implementation of the PCG algorithm outlined in the preceding section. Direct computation of the pressure-to-source operator $\Lambda^{\pm}_{z_s}$, for instance by solving 9 and reading off $P_s v^{\pm}_z$, turns out to be numerically ill-behaved. The relation 50 provides and alternative approach, taking advantage of the accurate approximate inverse to $S^+_{z_s,z_r}$ constructed above. The first row of 50, slightly rearranged, is

$$\Pi_0 \mathcal{S}^+_{z_s,z_r} \Pi_1^T f_s \approx -\frac{1}{2} S^+_{z_s,z_r} \Lambda^+_{z_s} f_s. \tag{67}$$

The approximate inverse construction for $S^+{}_{+z_s,z_r}$ permits (approximate) solution of this equation for $\Lambda^+_{z_s} f_s$: apply $4(V^+_{z_s,z_r})^T$ to both sides of equation 67 and use the first equation in the list **??** to get

$$\Lambda^+_{z_s} \approx -8(V^+_{z_s,z_r})^T \Pi_0 \mathcal{S}^+_{z_s,z_r} \Pi_1^T. \tag{68}$$

This identity is the major result of this section: it shows how to compute that action of $\Lambda^+_{z_s}$ by propagating the input pressure trace, identified as a source for the velocity evolution, forward in time from z_s to z_r reading off the pressure trace on $z = z_r$, identifying it once more as a point load (source for velocity), propagating it backwards in time from z_r to z_s, and finally reading off the velocity trace, interpreted as a pressure evolution source on z_s.

The importance of this result lies in the failure of the obvious method for computing the action of $\Lambda^{\pm}_{z_s}$, namely to employ the pressure trace as a source in the velocity equation (f_s, in the notation used above) at $z = z_s$, and read off the velocity field also at $z = z_s$. This difficulty is related to the existence of tangentially propagating waves and the lack of continuity of the trace operator. The method implicit in equation 68 avoids this difficulty by propagating the fields a positive distance in z: assuming as always that the causal fields are downgoing, this step eliminates any tangentially propagating fields from consideration.

A deeper study of the pressure-to-source operator (or of the closely related Dirichlet-to-Neumann operator for the second order wave equation, see Stefanov and Uhlmann (2005)) shows that it is approximately dependent only on the model coefficients near the source surface ($z = z_s$ in this case). Since the homogeneous and lens models are identical near this surface, it is unsurprising that these figures are very close to the previous two. However an even more useful observation is that the calculations in the approximation 68 could just as well be carried out in a much smaller region around the source surface, and produce a result that is functionally identical in that it will serve as a source for the same acoustic fields globally, with small error. In effect, equation 68 involving propagation from source ($z = z_s$) to receiver ($z = z_r$) surfaces is altered by replacing z_r with a receiver datum $z_s + \Delta z$ considerably closers to z_s:

$$\Lambda^+_{z_s} \approx -8(V^+_{z_s,z_s+\Delta z})^T \Pi_0 \mathcal{S}^+_{z_s,z_s+\Delta z} \Pi_1^T. \tag{69}$$

Using a receiver datum closer to the source surface has two favorable consequences:

- The computational domain can be smaller than is necessary to simulate the target data, as it need only contain the source surface and the receiver datum implicit in equation 68. This shrinkage of the computational domain can lead to substantial improvements in computational efficiency.
- Since the receiver data may be chosen much closer to the source surface that is the case for the target data, the effective aperture active in the relation 68 can be much larger, producing an estimated source gather much less affected by aperture limitation.

As mentioned in the last section, computation of the transpose of Λ^+ (exact, not approximate in the high frequency sense) is critical to the successful construction of the preconditioner. The relation 68 does not provide a computation for this operator. However set

$$\tilde{\Lambda}^+_{z_s} = -8(V^+_{z_s,z_s+\Delta z})^T \Pi_0 \mathcal{S}^+_{z_s,z_s+\Delta z} \Pi_1^T. \tag{70}$$

Then 69 can be rewritten

$$\Lambda^+_{z_s} \approx \tilde{\Lambda}^+_{z_s}.$$

Of course, all of the examples so far show images of $\tilde{\Lambda}^+_{z_s}$.

Since successful preconditioning requires only approximate inversion, use of $\tilde{\Lambda}^+_{z_s}$ in place of $\Lambda^+_{z_s}$ will still yield a working preconditioner, and the former can be transposed to machine precision via the definition 70 and the adjoint state method (equations **?? ??**):

$$(\tilde{\Lambda}^+_{z_s})^T = -8\Pi_1(\mathcal{S}^+_{z_s,z_s+\Delta z})^T \Pi_0^T V^+_{z_s,z_s+\Delta z} \tag{71}$$

The model space weight operator W_m^{-1} introduced in the last section is replaced by its asymptotic approximation

$$\begin{aligned}
&\frac{1}{2}(\tilde{\Lambda}^+_{z_s} + (\tilde{\Lambda}^+_{z_s})^T) \\
&\approx -8\left((V^+_{z_s,z_s+\Delta z})^T \Pi_0 \mathcal{S}^+_{z_s,z_s+\Delta z} \Pi_1^T + \right. \\
&\qquad \left. \Pi_1(\mathcal{S}^+_{z_s,z_s+\Delta z})^T \Pi_0^T V^+_{z_s,z_s+\Delta z}\right) \\
&= -4(\Pi_1(\mathcal{S}^+_{z_s,z_s+\Delta z})^T(\Pi_0^T\Pi_1 + \Pi_1^T\Pi_0)\mathcal{S}^+_{z_s,z_s+\Delta z}\Pi_1^T) = \tilde{W}_m^{-1}.
\end{aligned} \tag{72}$$

with a similar definition for the replacement $\tilde{W}_d$ of W_d.

This identity shows that only one forward and one adjoint simulation are necessary to compute the action of $\tilde{W}_{m,d}$. The operator in the center of the expression on the right-hand side, $\Pi_0^T\Pi_1 + \Pi_1^T\Pi_0$, simply exchanges the components of the acoustic fields, passing the velocity field as a pressure source and the pressure field as a velocity source.

One more computation is required for the full implementation of the preconditioning strategy explained in the last section: W_m is required, not just W_m^{-1}. Note that W_m plays two roles in the second term in equation 62: it is the weight matrix for both the domain and range norms for A. It is perfectly OK for one of these to be replaced by an asymptotic approximation, so long as it is symmetric and computable (and at least semi-definite). The second row in equation 50 appears as 51 above: introducing (formally) the inverse of Λ^+,

$$-\frac{1}{2}\Pi_1\mathcal{S}^+_{z_s,z_r}\Pi_0^T \approx V^+_{z_s,z_r}(\Lambda^+_{z_s})^{-1} \tag{73}$$

whence from the second line in display **??**

$$-\frac{1}{8}(S^+_{z_s,z_r})^T\Pi_1\mathcal{S}^+_{z_s,z_r}\Pi_0^T \approx (\Lambda^+_{z_s})^{-1} \tag{74}$$

and

$$-\frac{1}{8}\Pi_0(\mathcal{S}^+_{z_s,z_r})^T\Pi_1^T S^+_{z_s,z_r} \approx ((\Lambda^+_{z_s})^{-1})^T. \tag{75}$$

Using the definition 11 of $S^+_{z_s,z_r}$, the symmetrized Λ^{-1} is

$$\tilde{W}_m = -\frac{1}{16}\left(\Pi_0(\mathcal{S}^+_{z_s,z_r})^T(\Pi_1^T\Pi_0 + \Pi_0^T\Pi_1)\mathcal{S}^+_{z_s,z_r}\Pi_0^T\right) \approx \frac{1}{2}((\Lambda^+_{z_s})^{-1} + ((\Lambda^+_{z_s})^{-1})^T). \tag{76}$$

Comparison with the definition 72 shows that $\tilde{W}_m$ and $\tilde{W}_m^{-1}$ differ only in the initial and final projection factors (and overall scale), and in particular either can be computed for the cost of a forward/adjoint operator pair. Note that $\tilde{W}_m^{-1}$ is inverse to $\tilde{W}_m$ only in an approximate (asymptotic, aperture-limited) sense.

CONCLUSION

The linear modeling operator of surface source extended acoustic waveform inversion is approximately invertible, and this paper has shown how to approximately invert it. The construction is based on reverse time propagation of data, as inspired by the literature on photoacoustic tomography. However, since the input energy comes from a surface source, rather than a pressure boundary value, the pressure-to-source operator intervenes. It provides not just an approximate inverse, but a definition of weighted norms in domain and range spaces of the modeling operator, in terms of which that operator is approximately unitary. Accordingly, Krylov space iteration defined in terms of these weighted norms, or equivalently preconditioned Conjugate Gradient iteration, gives a rapidly convergent solution method for the linear subproblem.

The existence of an approximate unitary representation of the modeling operator is not merely a computational convenience, however. It reveals fundamental aspects of the operator's structure that enable an explanation for the mitigation of cycle-skipping, a feature of the *nonlinear* extended inverse problem. This fact echoes

earlier observations concerned a reflected wave inverse problem, involving a modeling operator with a similar approximate inverse (ten Kroode, 2014; Symes, 2014). Also, the approximate inverse leads to a stable computation of the gradient of the nonlinear objective function 4, resolving a difficulty first noted also for reflected wave inversion (Kern and Symes, 1994).

All of the topics treated here are open for elastic wave physics - the analogue of the pressure-to-source map would is the map from surface velocity field to corresponding constitutive defect, analogous to the elastic Dirichlet-to-Neumann map investigated by Rachele (2000).

The underlying tool in the ideas developed here is geometric optics (or ray theory), without which the very concept of downgoing waves would be meaningless. The physics of actual earth materials includes material heterogeneity on all scales, which appears to leave little room for the assumption of scale separation underlying geometric optics. Moreover, earth materials are anelastic, with elastic wave energy being converted to and from thermal excitation, pore fluid motion, and so on. A truly satisfactory understanding of inverse wave problems will eventually need to accommodate heterogenity and anelasticity beyond the current capabilities of the ray-based theory.

APPENDIX A

ADJOINT COMPUTATION

The adjoint of $\mathcal{S}^+_{z_s,z_r}$ can be computed by a variant of the adjoint state method, in this case a by-product of the conservation of energy. This calculation leads to equation **??**, from which the other statements about adjoints made in the second section of the paper follow.

Suppose that $p^-, \mathbf{v}^-$ solve 9 with $(h_s, f_s\mathbf{e_z})\delta(\mathbf{z}-\mathbf{z_s})$ replaced by $(h_r, f_r\mathbf{e_z})\delta(\mathbf{z}-\mathbf{z_r})$. Then

$$
\begin{aligned}
0 &= \left(\int dx\,dy\,dz\,\frac{p^+p^-}{\kappa} + \rho\mathbf{v}^+\cdot\mathbf{v}^-\right)|_{t\to\infty} - \left(\int dx\,dy\,dz\,\frac{p^+p^-}{\kappa} + \rho\mathbf{v}^+\cdot\mathbf{v}^-\right)|_{t\to-\infty} \\
&= \int_{-\infty}^{\infty} dt\,\frac{d}{dt}\left(\int dx\,dy\,dz\,\frac{p^+p^-}{\kappa} + \rho\mathbf{v}^+\cdot\mathbf{v}^-\right) \\
&= \int_{-\infty}^{\infty} dt\,\left(\int dx\,dy\,dz\,\frac{1}{\kappa}\frac{\partial p^+}{\partial t}p^- + p^+\frac{1}{\kappa}\frac{\partial p^-}{\partial t}\right. \\
&\qquad \left. + \rho\frac{\partial\mathbf{v}^+}{\partial t}\cdot\mathbf{v}^- + \rho\mathbf{v}^+\cdot\frac{\partial\mathbf{v}^-}{\partial t}\right) \\
&= \int_{-\infty}^{\infty} dt\,\left(\int dx\,dy\,dz\,\left(-\nabla\cdot\mathbf{v}^+ + h_s\delta(z-z_s)\right)p^- + p^+\left(-\nabla\cdot\mathbf{v}^- + h_r\delta(z-z_r)\right)\right. \\
&\qquad \left. + \left(-\nabla p^+ + f_s\mathbf{e_z}\right)\cdot\mathbf{v}^- + \mathbf{v}^+\cdot\left(-\nabla\mathbf{p}^- + \mathbf{f_r}\mathbf{e_z}\right)\right)
\end{aligned}
$$

$$= \int_{-\infty}^{\infty} dt \left(\int dx\, dy\, dz \, \left(-\nabla \cdot \mathbf{v}^+ + h_s \delta(z - z_s) \right) p^- + p^+ \left(-\nabla \cdot \mathbf{v}^- + h_r \delta(z - z_r) \right) \right.$$
$$\left. + p^+ (\nabla \cdot \mathbf{v}^-) + (\nabla \cdot \mathbf{v}^+) p^- + f_s \delta(z - z_s) v_z^- + v_z^+ f_r \delta(z - z_r) \right)$$

after integration by parts in the last two terms. Most of what is left cancels, leaving

$$0 = \int_{-\infty}^{\infty} dt\, dx\, dy \, (h_s P_s p^- + f_z P_s v_z^-) + (h_r P_r p^+ + f_r P_r v_z^+)$$
$$= \langle (h_s, f_s), \mathcal{S}^-(h_r, f_r) \rangle + \langle (h_r, f_r), \mathcal{S}^+_{z_s, z_r}(h_s, f_s) \rangle$$

whence **??** follows immediately.

DECLARATIONS

Funding

The author did not receive support from any organization for the submitted work.

Competing Interests

The author certifies that he has no affiliations with or involvement in any organization or entity with any financial interest or non-financial interest in the subject matter or materials discussed in this manuscript.

Data, Material, and Code Availability

The computational examples reported in this work were written in the Madacascar reproducible research framework (`http:www.reproducibility.org`). Code and data source is available from the author on request.

REFERENCES

Aghmiry, H., A. Gholami, and S. Operto, 2020, Accurate and efficient data-assimilated wavefield reconstruction in the time domain: Geophysics, **85**, no. 2, A7–A12.

Bao, G., and W. Symes, 1991, A trace theorem for solutions of linear partial differential equations: Mathematical Methods in the Applied Sciences, **14**, 553–562.

Courant, R., and D. Hilbert, 1962, Methods of mathematical physics, volume ii: Wiley-Interscience.

Dafni, R., and W. Symes, 2018, Accelerated acoustic least-squares inversion: 88th Annual International Meeting, Expanded Abstracts, Society of Exploration Geophysicists, 4291–4295.

Fichtner, A., 2010, Full seismic waveform modelling and inversion: Springer Verlag.

Gauthier, O., A. Tarantola, and J. Virieux, 1986, Two-dimensional nonlinear inversion of seismic waveforms: Geophysics, **51**, 1387–1403.

Golub, G. H., and C. F. van Loan, 2012, Matrix computations, 4th ed.: Johns Hopkins University Press.

Guasch, L., A. Calderón, M. Tang, P. Nachev, and M. Warner, 2020, Full-waveform inversion imaging of the human brain: NPJ Digital Medicine, **3**.

Guasch, L., M. Warner, and C. Ravaut, 2019, Adaptive waveform inversion: Practice: Geophysics, **84**, R447–R461.

Hou, J., and W. Symes, 2016a, Accelerating extended least-squares migration with weighted conjugate gradient iteration: Geophysics, **81**, no. 4, S165–S179.

———, 2016b, Accelerating least squares migration with weighted conjugate gradient iteration: 78th Annual International Conference and Exhibition, Expanded Abstract, European Association for Geoscientists and Engineers, P104.

Hristova, Y., 2009, Time reversal in thermoacoustic tomography - an error estimate: Inverse Problems, **25**, 055008.

Huang, G., R. Nammour, W. Symes, and M. Dolliazal, 2019, Waveform inversion by source extension: 89th Annual International Meeting, Expanded Abstracts, Society of Exploration Geophysicists, 4761–4765.

Kern, M., and W. Symes, 1994, Inversion of reflection seismograms by differential semblance analysis: Algorithm structure and synthetic examples: Geophysical Prospecting, **99**, 565–614.

Lasiecka, I., 1986, Sharp regularity results for mixed hyperbolic problems of second order: Springer Verlag, volume **1223** *of* Springer Lecture notes in Mathematics.

Lasiecka, I., J.-L. Lions, and R. Triggiani, 1986, Non-homogeneous boundary value problems for second order hyperbolic operators: Journal de Mathématiques Pures et Appliquées, **65**, 149–192.

Lasiecka, I., and R. Trigianni, 1989, Trace regularity of the solutions of the wave equation with homogeneous boundary conditions and compactly supported data: Journal of Mathematical Analysis and Applications, **141**, 49–71.

Lax, P. D., 2006, Hyperbolic partial differential equations (Courant Lecture Notes): American Mathematical Society.

Li, Z., Y. Lin, and K. Zhang, 2018, Time-domain wavefield reconstruction inversion: Applied Geophysics, **14**, 523—-528.

Louboutin, M., G. Rizzuti, and F. Herrmann, 2020, Time-domain wavefield reconstruction inversion in a tti medium. (arXiv:2004.07355v1).

Payne, L., 1975, Improperly posed problems in partial differential equations: Lecture Note 22, CBMS, Society for Industrial and Applied Mathematics, Philadelphia.

Pladys, A., R. Brossier, Y. Li, and L. Métivier, 2021, On cycle-skipping and misfit function modification for full-wave inversion: Comparison of five recent approaches: Geophysics, **86**, R563–R587.

Plessix, R.-E., 2006, A review of the adjoint-state method for computing the gradient

of a functional with geophysical applications: Geophysical Journal International, **167**, 495–503.

Rachele, L., 2000, Boundary determination for an inverse problem in elastodynamics: Communications in Partial Differential Equations, **25**, 1951–1996.

Schuster, G., 2017, Seismic inversion: Society of Exploration Geophysicists. Investigations in Geophysics.

Stefanov, P., and G. Uhlmann, 2005, Stable determination of generic simple metrics from the hyperbolic Dirichlet-to-Neumann map: International Mathematics Research Notices, **17**, 1047–1061.

———, 2009, Thermoacoustic tomography with variable sound speed: Inverse Problems, **25**, 075011.

Symes, W., 2014, Seismic inverse problems: recent developments in theory and practice: Inverse Problems - from Theory to Application, Proceedings, Institute of Physics, 2–5.

Symes, W., H. Chen, and S. Minkoff, 2020, Full waveform inversion by source extension: why it works: 90th Annual International Meeting, Expanded Abstracts, Society of Exploration Geophysicists, 765–769.

Symes, W., and L. E. Payne, 1983, Trace theorem for solutions of the wave equation and the remote determination of acoustic sources: Mathematical Methods in the Applied Sciences, **5**, 131–152.

Tang, B., S. Xu, and Y. Zhang, 2013, 3D angle gathers with plane-wave reverse time migration: Geophysics, **78**, no. 2, S117–S123.

ten Kroode, F., 2012, A wave-equation-based Kirchhoff operator: Inverse Problems, 115013:1–28.

———, 2014, A Lie group associated to seismic velocity estimation: Inverse Problems - from Theory to Application, Proceedings, Institute of Physics, 142–146.

van Leeuwen, T., and F. Herrmann, 2013, Mitigating local minima in full-waveform inversion by expanding the search space: Geophysical Journal International, **195**, 661–667.

———, 2016, A penalty method for pde-constrained optimization in inverse problems: Inverse Problems, **32**, 1–26.

Virieux, J., and S. Operto, 2009, An overview of full waveform inversion in exploration geophysics: Geophysics, **74**, no. 6, WCC127–WCC152.

Warner, M., and L. Guasch, 2016, Adaptive waveform inversion: theory: Geophysics, **81**, R429–R445.

Warner, M., T. Nangoo, A. Umpleby, N. Shah, D. Kahn, and M. Isernia, 2021, Adaptive reflection waveform inversion: Faster, tighter, deeper, smarter: 91st Annual International Meeting, Expanded Abstracts, Society of Exploration Geophysicists, 582–586.

Xu, S., D. Wang, F. Chen, G. Lambaré, and Y. Zhang, 2012, Inversion on reflected seismic wave: SEG Technical Program Expanded Abstracts, 1–7.

Xu, S., Y. Zhang, and B. Tang, 2011, 3D angle gathers from reverse time migration: Geophysics, **76**, no. 2, S77–S92.

Yong, P., R. Brossier, L. Métivier, Y. Li, W. He, and J. Virieux, 2021, Improving adaptive waveform inversion by local matching filter: 82nd EAGE Annual Confer-

ence and Exhibition, Expanded Abstracts, European Association of Geoscientists and Engineers, 1–5.

Zhang, Y., A. Ratcliffe, G. Roberts, and L. Duan, 2014, Amplitude-preserving reverse time migration: from reflectivity to velocity and impedance inversion: Geophysics, **79**, S271–S283.

Zhang, Y., and J. Sun, 2009, Practical issues of reverse time migration: True amplitude gathers, noise removal and harmonic-source encoding: Beijing International Geophysical Conference and Exposition, Expanded Abstracts, Society of Exploration Geophysicists, 204–209.